JGR Space Physics

Key Points:

- Reconnection current sheets form at the Q-⊥per bow shock by the compression of an interplanetary RD as it interacts with the shock
- The evidence of reconnection includes the formation of flux ropes, high-speed outflows, and Hall magnetic and electric fields
- More reconnection sites inside the RD current layer are found in the magnetosheath downstream of the Q-⊥per shock

Correspondence to:
Z. Guo,
guozf@mail.iggcas.ac.cn

Magnetic Reconnection Inside Solar Wind Rotational Discontinuity During Its Interaction With the Quasi-Perpendicular Bow Shock and Magnetosheath

Zhifang Guo[1,2,3] , **Yu Lin[3]** , **Xueyi Wang[3]** , and **Aimin Du[1,2,4]**

[1]Key Laboratory of Earth and Planetary Physics, Institute of Geology and Geophysics, Chinese Academy of Sciences, Beijing, China, [2]Innovation Academy for Earth Science, Chinese Academy of Sciences, Beijing, China, [3]Physics Department, Auburn University, Auburn, AL, USA, [4]College of Earth and Planetary Sciences, University of Chinese Academy of Sciences, Beijing, China

Abstract Using a three-dimensional global hybrid simulation, we investigate the formation and evolution of ion-scale magnetic reconnection inside an interplanetary rotational discontinuity (RD) owing to its interaction with the quasi-perpendicular (Q-⊥) bow shock and the magnetosphere. The interplanetary magnetic field (IMF) is initially predominantly northward, while it changes to purely southward across the RD. A significantly thinned RD current layer with a width ∼ ion skin depth and normal magnetic field $B_n \approx 0$ is formed by a shock compression process as the RD interacts with the Q-⊥ shock. Magnetic reconnection thereupon takes place inside the thin RD current layer, where Hall magnetic and electric fields, reconnection electric field, and high-speed ion outflow jets are identified. Simultaneously, flux ropes form with an extension of a few ion inertial lengths. As the RD is transmitted into the magnetosheath, multiple reconnection sites lead to the formation of longer flux ropes. Moreover, magnetosheath reconnection is also found at new reconnection sites inside the RD. No reconnection is found in the Q-⊥ shock alone outside the RD. The flux ropes propagate poleward and tailward in the magnetosheath. In addition, magnetopause reconnection takes place under the southward IMF on the sunward side of the RD after the RD passes through the magnetopause.

1. Introduction

The terrestrial magnetopause, magnetosheath, and bow shock provide a unique platform to understand the interaction among the solar wind, bow shock, and the magnetosphere. Magnetic reconnection is known to be a fundamental plasma process in such interaction (e.g., Dungey, 1961). This key process is not only regarded to offer a dominant mechanism for the entry of solar wind plasma into the magnetosphere at the magnetopause (e.g., Burch et al., 2016; Hasegawa et al., 2010; Mozer et al., 2002; Paschmann et al., 1979; Phan et al., 2004), but it has also been identified to play an important role in the plasma heating and acceleration at the bow shock (e.g., Hamrin et al., 2019) and in the magnetosheath (e.g., Lu et al., 2020; Øieroset et al., 2017; Phan et al., 2018; Retinò et al., 2007).

Around the dayside magnetopause, two types of reconnection current sheets are observed in general according to their location and origin. One is generated locally at the magnetopause or in the turbulent magnetosheath, and the other is present in discontinuities that are transmitted from the solar wind through the bow shock. When the interplanetary magnetic field (IMF) points southward, reconnection is observed at the dayside magnetopause (e.g., Cooling et al., 2001; Guo et al., 2021; Moore et al., 2002; Sonnerup et al., 1981; Trattner et al., 2007). Under a northward IMF condition, reconnection current sheets can be generated locally tailward of the cusp (e.g., Fuselier et al., 2012; Onsager et al., 2001). Evidence of the magnetosheath reconnection on the ion scales has been observed by the MMS (e.g., Eastwood et al., 2018; Phan et al., 2018; Vörös et al., 2017; Yao et al., 2020; Yordanova et al., 2016), THEMIS (e.g., Øieroset et al., 2017), and Cluster (e.g., Retinò et al., 2007) spacecraft. Recently, reconnection current layers on the electron-kinetic scales have also been observed around the quasi-parallel (Q-∥) shock (Gingell et al., 2019; Wang et al., 2018). It is suggested that the reconnection current sheets form spontaneously in the turbulent plasma of the Q-∥ shock.

On the other hand, reconnection has also been observed inside solar wind discontinuities as they interact with the bow shock (e.g., Hamrin et al., 2019; Maynard et al., 2007; Phan et al., 2007, 2011). The solar wind discontinuities are very common structures in space plasmas (e.g., Behannon et al., 1981; Burlaga et al., 1977; Lepping

& Behannon, 1986; Tsurutani & Smith, 1979). Among them, the discontinuities with a significant change in the magnetic field direction are frequently observed. These discontinuities are referred to as directional discontinuities (DDs), including rotational discontinuities (RDs), and directional tangential discontinuities (TDs). Based on multispacecraft observations, Phan et al. (2007) and Maynard et al. (2007) found reconnection events in the magnetosheath after a nonreconnecting interplanetary current sheet crossed the bow shock. Phan et al. (2011) reported that a reconnecting current sheet in a solar wind discontinuity stopped reconnection in the magnetosheath but then possessed reconnection again at a later stage near the magnetopause. Hamrin et al. (2019) suggested that reconnection can take place at the quasi-perpendicular (Q-⊥) bow shock because of the compression of a directional discontinuity at the bow shock. More recently, Kropotina et al. (2021) showed that the bow shock-RD interaction may alter the properties of the RD, which in turn makes the RD unstable to magnetic reconnection. Nevertheless, it is often hard for space observations to conclude whether reconnection has taken place inside the discontinuity before or after it touches with the bow shock.

Numerical simulations were performed to explore the interaction of dayside plasma regions with interplanetary discontinuities from the solar wind. Using two-dimensional (2D) (Lin, 1997; Omidi et al., 2009 and three-dimensional (3D) (Pang et al., 2010) global hybrid simulations, magnetic reconnection was found inside a TD current layer in the Q-⊥ magnetosheath due to the interaction between the TD and the bow shock. The 3D global hybrid simulation of Guo et al. (2018, 2021a) found that reconnection can take place in both the Q-⊥ and the Q-∥ bow shock and the downstream magnetosheath during the TD-bow shock-magnetosheath interaction, leading to flux ropes in the magnetosheath, which subsequently impact the magnetopause. Recently, using again a 3D global hybrid simulation, Guo et al. (2021b) found that reconnection on the ion-kinetic scales can be triggered inside an RD in the Q-∥ magnetosheath as the RD current layer is altered by the turbulent low-frequency waves during its interaction with the Q-∥ shock.

Nevertheless, unlike the Q-∥ magnetosheath, waves in the Q-⊥ magnetosheath are relatively weak (e.g., Eastwood et al., 2005; Lee & Russell, 1994; Liu et al., 2018). It is still unclear how interplanetary RDs interact with the Q-⊥ shock, and what is the subsequent evolution of the RDs in the dayside magnetosheath. Moreover, different from TDs, a normal component of the magnetic field, B_n, exists in RDs. A specific question is: Can reconnection occur when the RD interacts with the Q-⊥ bow shock-magnetosphere system? The purpose of this manuscript is to address this question by investigating the RD-bow shock-magnetosphere interaction under the Q-⊥ shock geometry.

In this paper, we investigate the RD-bow shock-magnetosphere interaction with our 3D self-consistent global-scale hybrid simulation. We first show that reconnection can take place inside the RD after it is compressed by the Q-⊥ shock. The formation and evolution of reconnection and twisted flux ropes as well as the subsequent impacts of the RD on the magnetopause are then investigated. The remainder of this paper is structured as follows. In Section 2, we present a brief overview of the simulation model. Section 3 then describes our simulation results. Finally, Section 4 presents the conclusion and discussion.

2. Simulation Model

Our simulation uses the 3D global-scale hybrid code of Lin and Wang (2005) for the dayside magnetosphere. Details of the simulation scheme have been described by Swift (1996). The same code has been utilized in our previous studies of the interaction between solar wind directional discontinuities and the dayside magnetospheric system (Guo et al., 2018, 2021a, 2021b). In the hybrid scheme, ions are treated as fully kinetic particles, whereas electrons are treated as a massless fluid. To better model the curved dayside magnetosphere and the bow shock, a spherical coordinate system (r, θ, φ) is adopted, where the longitudinal angle (φ) is the angle made from the geocentric solar magnetospheric (GSM) y axis and the polar angle (θ) is the angle from the GSM z axis. The simulation domain contains the dayside plasma regions within $3.5R_E \leq r \leq 25R_E$, where R_E denotes the Earth's radius. The 3D cell grid number is chosen as $N_r \times N_\theta \times N_\varphi = 380 \times 220 \times 260$. The grids in the r direction are nonuniformly distributed, while uniform grids are used in the θ and φ directions. A higher spatial resolution is used around the bow shock, magnetosheath, and magnetopause, with a grid size of $\Delta r \approx 0.025R_E$. About 150–600 ion particles are used per cell.

In the simulation, the magnetopause, magnetosheath, and bow shock form self-consistently as the supersonic solar wind crashes into the terrestrial dipole magnetic field. The solar wind inflow conditions are imposed at the
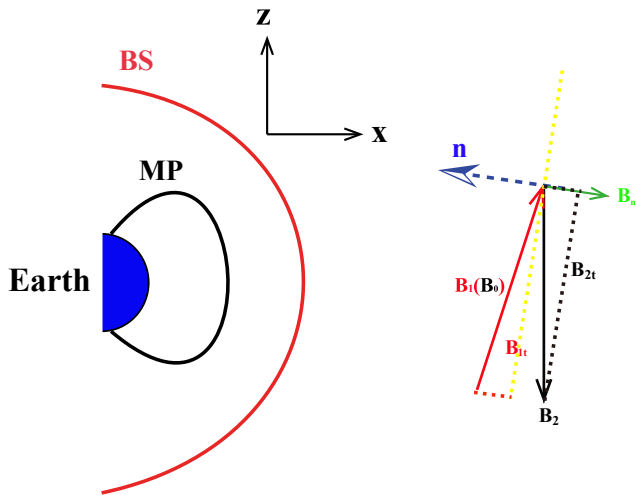
Figure 1. A depiction of the magnetic field direction variation in xz plane across the RD. B_1 (B_0) is the RD upstream magnetic field and B_2 is the RD downstream magnetic field. The angle between B_1 and B_2 is θ_{12}. The propagation direction of the RD is $n = (-\sin(\theta_{12}/2), 0, -\cos(\theta_{12}/2))$.

outer boundary of $r = 25R_E$. Open boundary conditions are utilized at the outflow boundary of $x = 0$. Perfectly conducting boundary conditions are utilized at the inner boundary of $r = 3.5R_E$.

In the cases presented, the IMF is assumed to have a magnitude of $B_0 = 10nT$. The corresponding ion gyrofrequency $\Omega_{i0} = eB_0/m_i$ is $\sim 1.0s^{-1}$. To save computational cost, a larger ion inertial length $d_{i0} = 0.1R_E$ of the solar wind is chosen. To resolve the ion-scale physics, the grid sizes used in our simulation are less than the local ion gyro-radius (ρ_i) or the ion inertial length (d_i) (e.g., Lin et al., 2014). For example, the ion density N_i increases to $\sim 4N_0$ in the magnetosheath (where, N_0 is the ion density in the solar wind), corresponding to a local ion inertial length $\sim 0.05R_E$. The grid size $\Delta r \approx 0.025R_E$ is chosen in this region. The anomalous resistivity is set as $v = 0.02\Omega_i J/J_0$, which is dependent upon the current density J, where $J_0 = B_0/\mu_0 d_{i0}$. In the presentation below, all variables are normalized to the corresponding parameters in the unperturbed solar wind. For example, the ion density N_0, magnetic field B_0, Alfvén speed V_{A0} (where, $V_{A0} = B_0/\sqrt{\mu_0 m_i N_0}$), and the ion gyro-frequency Ω_{i0}^{-1} in the solar wind are the normalization units of the ion number density N_i, magnetic field strength B, plasma velocity V, and time t, respectively.

To study the RD-bow shock-magnetosphere interaction, the bow shock must completely form before an interplanetary RD enters the simulation domain. In addition, we assume that the initial IMF has a dominant northward B_z component, corresponding to a Q-⊥ bow shock geometry. The ion and electron plasma beta values in the solar wind are chosen as $\beta_i = \beta_e = 0.5$. The solar wind Alfvén Mach number is chosen as $M_A = V_{sw}/V_{A0} = 5.6$, where V_{sw} is the solar wind flow speed. The RD has an initial half-width of $1d_{i0}$, and its propagation direction is set as $n = (-0.996, 0, 0.087)$. Across the RD, the plasma density and pressure are constant. The normal magnetic field B_n is constant. The strength of the tangential magnetic field remains constant, while the direction is assumed to change by a rotation angle of $\Delta\Phi = 180°$. The normal flow velocity V_n is constant across the RD, and the tangential velocity V_t varies according to the Walén relation. Detailed descriptions of how the interplanetary RD is imposed in the simulation can be referred to Guo et al. (2021b).

The GSM coordinate system is adopted in the presentation of the simulation results. Figure 1 schematically shows the magnetic field direction variation in the xz plane across the RD. The upstream (earthward side) magnetic field of the RD is denoted by B_1, and its downstream magnetic field is marked by B_2. The quantities B_t and B_n are the tangential and normal magnetic fields, respectively. The initial IMF, $B_0 = B_1$, is assumed to be $(0.174, 0, 0.985)B_0$. For the case shown in the paper (Figure 1), the downstream magnetic field of the RD points purely southward, with $B_2 = (0, 0, -1.0)B_0$. The angle between B_1 and B_2 across the RD is $\theta_{12} = 170°$, similar to the MMS event observed by Hamrin et al. (2019). Across the RD, the solar wind velocity V_{sw} changes from $(-5.62, 0, 0)V_{A0}$ to $(-5.79, 0, -1.98)V_{A0}$.

3. Simulation Results

As reflected in Figure 1, the magnetic field is set to be $(B_{0x}, B_{0y}, B_{0z}) = (0.174, 0, 0.985)B_0$ on the earthward of the interplanetary RD, which is the initial IMF. At $t \approx 25\Omega_{i0}^{-1}$, the bow shock and the magnetopause have well developed in a self-consistent manner, where the magnetopause is located at x $\approx 10.0R_E$ and the bow shock is centered at x $\approx 12.8R_E$ around the subsolar region. Note that the bow shock is a Q-⊥ shock in most of the dayside region. At $t \approx 27\Omega_{i0}^{-1}$, the RD touches the inflow boundary at $(x, y, z) = (24.82, 0, -1.71)R_E$ and propagates into the simulation domain subsequently.

To show the spatiotemporal evolution of the RD as it moves through the dayside magnetosphere, Figures 2a–2e depict magnetic field lines projected in the $y = 0$ plane (marked by black lines) at $t = 40\Omega_{i0}^{-1}$, $50\Omega_{i0}^{-1}$, $55\Omega_{i0}^{-1}$, $60\Omega_{i0}^{-1}$, and $100\Omega_{i0}^{-1}$. The contour plots in the $y = 0$ plane show the magnitude of the magnetic field, B. Magnetic islands associated with magnetic flux ropes are present, marked by the colored circles in the 2D plane. The flux ropes are identified by tracing the 3D field lines. The bow shock is located at where the magnetic field strength
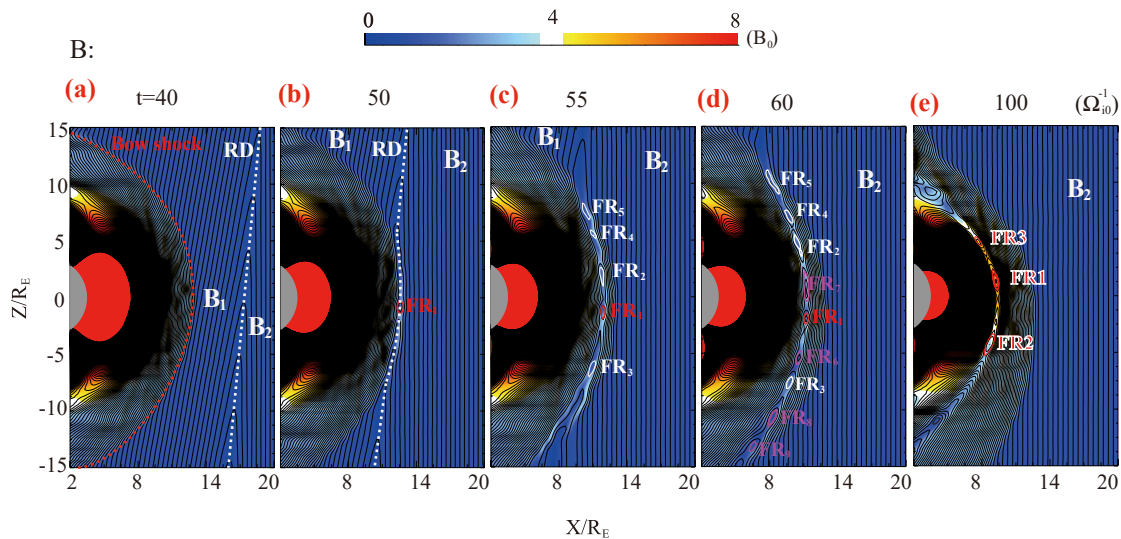
Figure 2. Contour plots of the magnetic field intensity B in the $y = 0$ plane, obtained at (a) $t = 40\Omega_{i0}^{-1}$, (b) $50\Omega_{i0}^{-1}$, (c) $55\Omega_{i0}^{-1}$, (d) $60\Omega_{i0}^{-1}$, and (e) $100\Omega_{i0}^{-1}$. The projection of the magnetic lines in the $y = 0$ plane is marked by the black lines. The white, pink, and red circles denote the magnetic flux ropes.

and particle density increase significantly, marked by the red dashed curve in Figure 2a. The RD has moved to the frontside of the bow shock at $t = 40\Omega_{i0}^{-1}$, as indicated by the dashed white line. As in the initial setup, the magnetic field changes from $(B_{1x}, B_{1y}, B_{1z}) = (0.174, 0, 0.985)B_0$ to $(B_{2x}, B_{2y}, B_{2z}) = (0., 0., -1.0)B_0$ across the RD in the sunward direction. No reconnection is seen before the RD hits the Q-⊥ bow shock. At the subsequent time $t = 50\Omega_{i0}^{-1}$, the RD (shown by the curved white dashed line in Figure 2b) has reached and interacted with the bow shock. At this moment, a flux rope marked by the red label "FR$_1$" is observed inside the RD.

As the RD is further transmitted through the bow shock, more flux ropes appear in the RD current layer. At $t = 55\Omega_{i0}^{-1}$, four new flux ropes (FR$_2$-FR$_5$) are present in the RD current layer, as denoted by the white labels "FR$_2$"-"FR$_5$," in Figure 2c. At $t = 60\Omega_{i0}^{-1}$, four more flux ropes have formed, denoted by the purple labels "FR$_6$"-"FR$_9$," in Figure 2d. These flux ropes subsequently move poleward and tailward with the magnetosheath flows. When the southward magnetic field behind the RD interacts with the magnetopause, reconnection occurs at the magnetopause, causing the generation of three magnetopause flux ropes at $t = 100\Omega_{i0}^{-1}$, as denoted by "FR1," "FR2," and "FR3" in Figure 2e. In the following subsections, detailed physical processes of the 3D reconnection associated with the RD and the southward IMF behind the RD are presented.

3.1. Reconnection Inside the RD

3.1.1. At the Bow Shock

Different from the interaction between an RD and the Q-∥ bow shock (Guo et al., 2021b), the generation of reconnection shown in Figure 2 is found to be due to a simple compression of the RD during its interaction with the Q-⊥ shock. To illustrate the evolution of the magnetic field line configuration of the RD, Figures 3a–3f depict the 3D perspective views of magnetic field lines around the RD at $t = 40\Omega_{i0}^{-1}$, $47\Omega_{i0}^{-1}$, and $50\Omega_{i0}^{-1}$. The magnetic field strength B in the $y = 0$ plane is superimposed in Figures 3a–3c. The field lines in an enlarged view are highlighted in Figures 3d–3f. The red lines represent the flux rope "FR$_1$," shown in Figure 2b. The field lines of the RD are denoted by the orange lines. As shown in Figures 3a and 3d, reconnection is not seen before the RD interacts with the Q-⊥ shock. The frontside of the RD has reached the Q-⊥ shock at $t = 47\Omega_{i0}^{-1}$, as shown by the red circle in Figures 3b and 3e. It is found that the field lines on the earthward side (upstream) and sunward side (downstream) of the RD bend slightly toward the duskside and dawnside, respectively, as a result of the compression process at the Q-⊥ bow shock. At $t = 50\Omega_{i0}^{-1}$, the transmitted RD is the thinnest, with a half-width of $\sim 0.33d_{i0}$, around $(x, y, z) = (12.71, 0, -1.69)R_E$, where it was first in contract with the Q-⊥ shock and compressed by the shock compression process (Guo et al., 2018; Pang et al., 2010). In the meantime, a localized looped magnetic flux rope ("FR$_1$") is found in the RD current layer, centered at $(x, z) = (12.73, -1.03)R_E$ in the $y = 0$ plane, whose length in the y direction is $\sim 15d_{i0}$ (Figures 3c and 3f). The reconnection site at $(x, z) = (12.71, -1.69)R_E$ on the southward
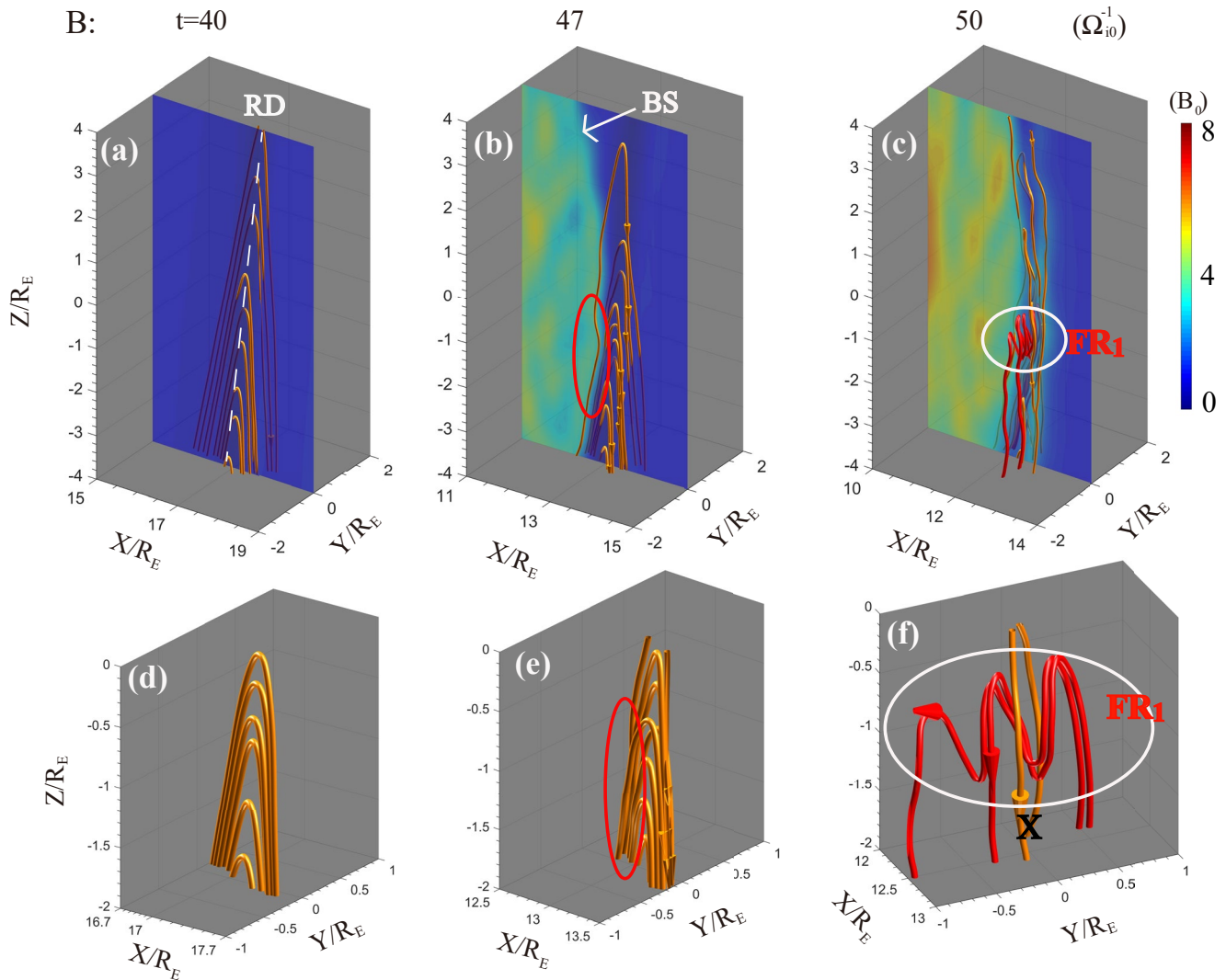
Figure 3. 3D global perspective views of the RD magnetic field lines marked by the orange lines at (a and d) $t = 40\Omega_{i0}^{-1}$, (b and e) $47\Omega_{i0}^{-1}$, and (c and f) $50\Omega_{i0}^{-1}$. Contours plots in the $y = 0$ plane are the magnitude of the magnetic field, B. The flux ropes at the Q-⊥ shock are marked by the red field lines.

side of "FR₁" is marked by the symbol "X" (Figure 3f). It is found that the Walén relation is not satisfied anymore at the RD locations across the reconnection site.

The formation of flux rope "FR₁" marked in Figure 3 when it was at the bow shock is investigated now. The magnetic field lines around "FR₁" at $t = 50\Omega_{i0}^{-1}$ are depicted in Figure 4a, and some zoom-in views of the field lines around the X lines are shown in Figures 4b and 4c. The green, blue, and white lines represent the magnetic field lines before reconnection occurs around the magnetic merging layer, and the orange lines are the reconnected ones. The red and black lines mark the twisted field lines (flux rope) after reconnection. Note that the normal magnetic field $B_n \approx 0$ in the thin current sheet before reconnection. The reconnection "X" point between the blue and white field lines is denoted by the black symbol "X," which is also marked in Figure 3f. In Figure 4b, reconnection has occurred between the white and blue field lines, producing the black and orange field lines. In the meantime, more subsequent reconnection also occurs between the green field line and black field line, leading to the formation of the orange and red field lines (Figure 4c). A new reconnection X point at $(x, y, z) = (12.7, -0.5, -1.67)R_E$ is denoted by the blue symbol "X." A reconnection X line is formed, which is through the reconnection X points in Figures 4b-4c, marked by the white dashed line in Figure 4a.

To provide the evidence of magnetic reconnection occurring at the black "X" point in Figure 4b, Figure 5 displays the contour plots of various physical quantities in a zoom-in view, including (a) the current density J_y,
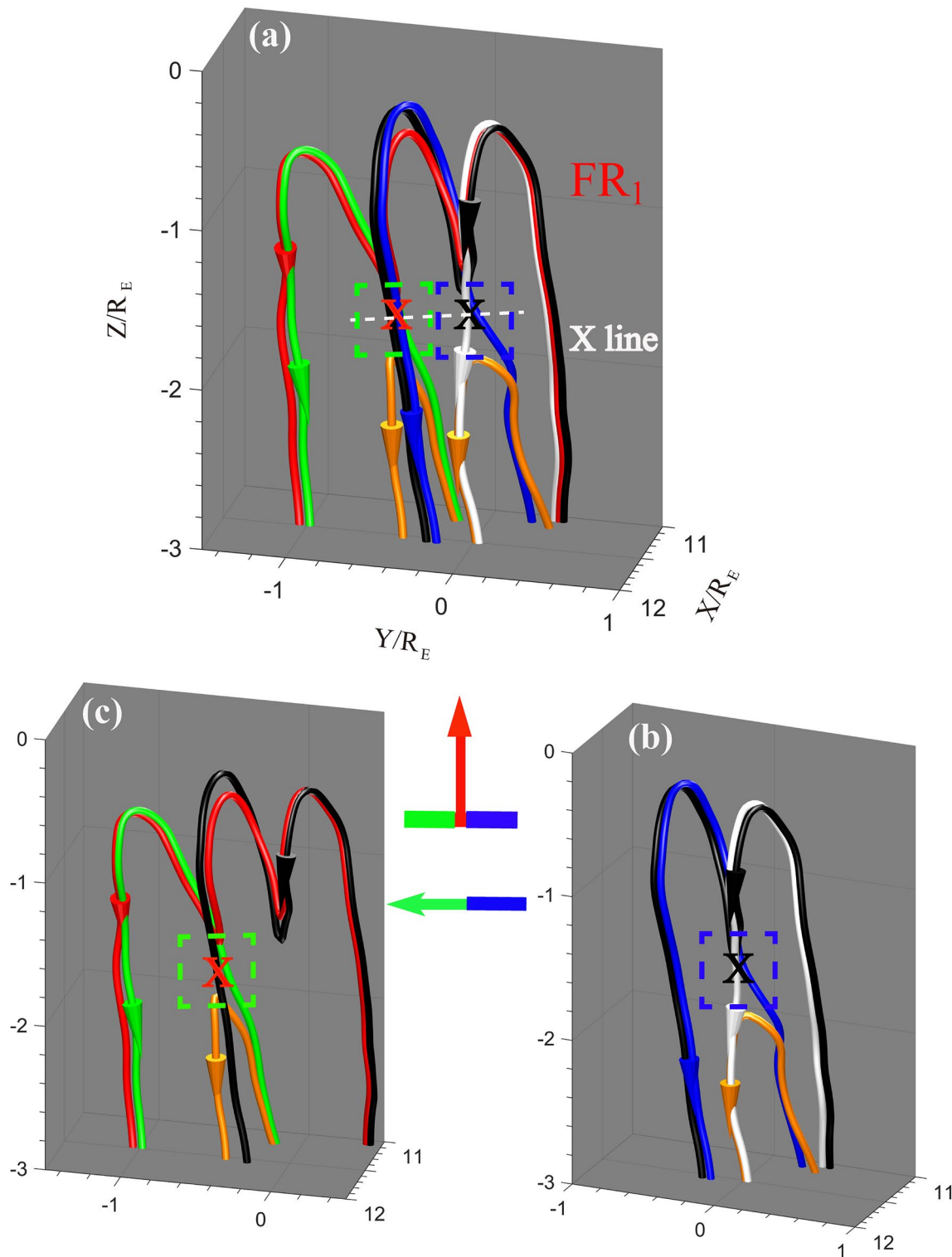
Figure 4. (a–c) Magnetic field lines around "FR$_1$" in an enlarged view at $t = 50\Omega_{i0}^{-1}$. The blue, green, and white lines represent the magnetic field lines of the RD before reconnection occurs, the orange lines are the reconnected field lines around the reconnection "X" points, and the black and red lines denote the twisted field lines of "FR$_1$".

$t=50\Omega_{i0}^{-1}$:
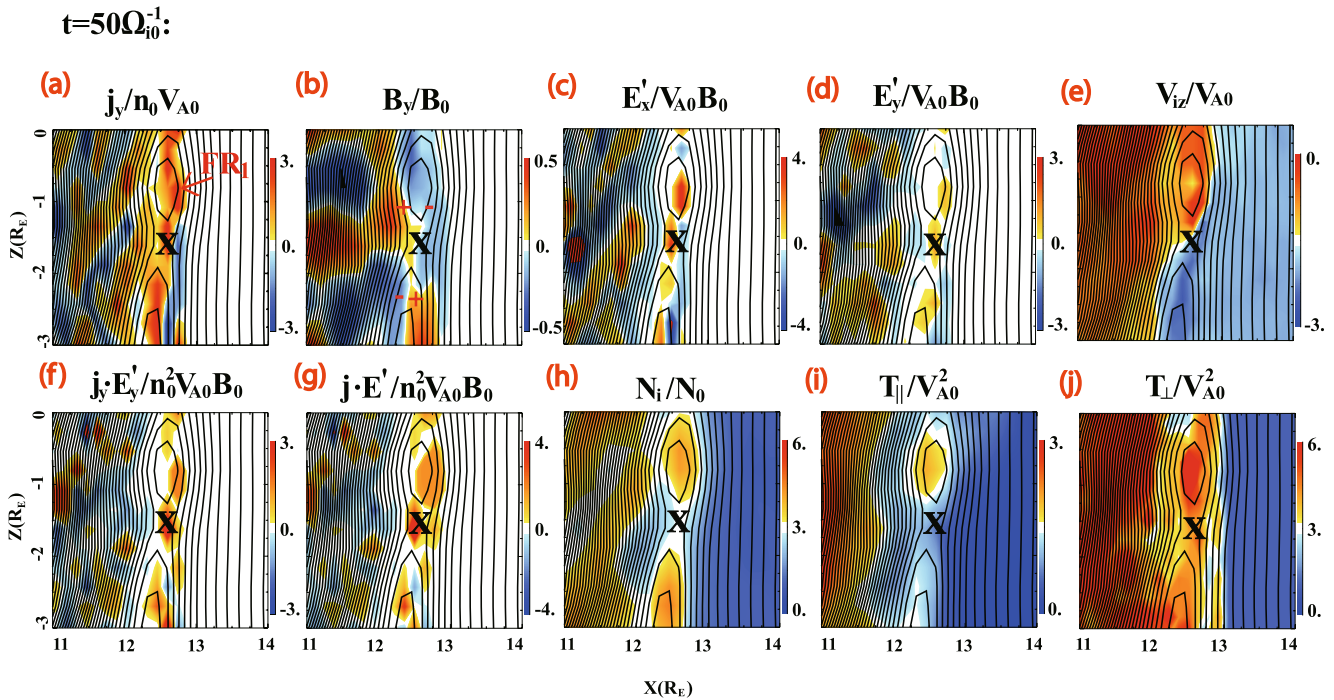
Figure 5. Zoom-in views of various physical quantities around "FR$_1$," including (a) the current density J$_y$, (b) the magnetic field B$_y$, (c) the Hall electric field $E'_x = E_x + (V_i \times B)_x$, (d) the reconnection electric field $E'_y = E_y + (V_i \times B)_y$, (e) the ion flow velocity component V$_{iz}$, (f) J$_y \cdot E'_y$, (g) J $\cdot$ E', (h) the ion density N_i, (i) the ion parallel temperature $T_{||}$, and (j) the ion perpendicular temperature $T_\perp$ in the y = 0 plane, within $x = 11R_E - 14R_E$ and $z = -3R_E - 0$, at $t = 50\Omega_{i0}^{-1}$.

(b) the magnetic field B$_y$, (c) the Hall electric field $E'_x = E_x + (V \times B)_x$, (d) the reconnection electric field $E'_y = E_y + (V \times B)_y$, (e) the ion flow velocity component V$_{iz}$, (f) $J_y \cdot E'_y$, (g) J $\cdot$ E', (h) the ion density N_i, (i) the ion parallel temperature $T_{i||}$, and (j) the ion perpendicular temperature $T_{i\perp}$ in the y = 0 plane, within $x = 11R_E - 14R_E$ and $z = -3R_E - 0$, at $t = 50\Omega_{i0}^{-1}$. Based on Figure 5a, a current sheet with a half-width of $\sim0.6d_i$ ($d_i \sim 0.56d_{i0}$ is the local ion inertial length) is present at $(x, z) = (12.71, -1.69)R_E$, as seen in the structure of the enhanced J$_y$. This current sheet is the RD being compressed by the shock compression process (Guo et al., 2018; Pang et al., 2010), from the upstream half-width of $\sim1.0d_{i0}$. The current density J$_y$ in the RD increases from $\sim0.3n_0V_{A0}$ in the solar wind to $\sim3.2n_0V_{A0}$ in the vicinity of the Q-$\perp$ bow shock. Around the reconnection "X" point, the guide field B_G (in the y-component) is $\sim0.2B_0$ and the magnetic field B_R is approximately $B_z \approx 3.0B_0$. Figure 5b reveals that quadrupolar magnetic perturbations are present, denoted by the signs of positive and negative δB_y, which is due to the Hall effects caused by the ion inertia (e.g., Pritchett, 2001). In addition, the Hall magnetic field perturbations with $\delta B_y \sim 0.5B_0$ are a little larger on the solar wind side than on the magnetosheath side ($\delta B_y \sim 0.3B_0$). Moreover, the thickness of the δB_y structure is wider on the sunward side than the earthward side. They are corresponding to an asymmetric reconnection with a smaller density on the sunward side. Reconnection in an asymmetric current sheet has been observed at the magnetopause (e.g., Birn et al., 2008; Pritchett, 2008) and at the Q-$\perp$ shock (e.g., Hamrin et al., 2019).

Figure 5c depicts that the E'_x structure caused by the Hall effect changes from negative on the sunward side to positive on the earthward side of the "X" point. In addition, the perturbation of E'_y with a magnitude of $\sim0.56V_{A0}B_0$ is found around the "X" point (Figure 5d). In Figure 5e, plasma jets V_{iz} in opposite directions are present in the reconnection outflow areas. Note that the ambient magnetosheath plasma flows move southward, with a speed is $\sim 2.0V_{A0}$. The outflow velocity south of the reconnection site is $\sim-2.7V_{A0}$, and it is $\sim-1.2V_{A0}$ on the northward side. Therefore, the outflow jets have a speed of $\sim 0.43V_A$ ($V_A \sim 1.74V_{A0}$ is local Alfven speed) relative to the X lines.

As shown in Figures 5f and 5g, positive values of $J_y \cdot E'_y$ and J $\cdot$ E' are present around the "X" point, indicating that the magnetic energy is being converted to the particle kinetic energy through the reconnection process. The ion density N_i inside the flux rope "FR$_1$" and at the outflow region has a significant enhancement in Figure 5h.

For the areas where the ion density N_i increases, Figures 5i and 5j show that ion temperatures $T_{i\parallel}$ and $T_{i\perp}$ are also enhanced. The ion density is about $\sim 3.0 N_0$ around the "X" point. As a result, the reconnection rate is about $E'_y / V_A B_R \sim \frac{E'_y}{V_{A0} B_0} \times \frac{B_0^2}{B_z^2} \times \sqrt{\frac{N_i}{N_0}} \simeq 0.11$, where $V_A = B_R / \sqrt{\mu_0 m_i N_i}$.

3.1.2. In the Magnetosheath

After the RD crosses the Q-$\perp$ shock, magnetosheath reconnection in the transmitted RD current layer is also generated. Figure 6 displays the magnetic field strength B in the $y = 0$ plane at (6a) $t = 55 \Omega_{i0}^{-1}$ and (6b) $t = 60 \Omega_{i0}^{-1}$. The colored lines superimposed on the contours show the flux ropes, while the corresponding field lines at $t = 55 \Omega_{i0}^{-1}$ and $t = 60 \Omega_{i0}^{-1}$ are depicted in Figures 6a1, 6a2, 6b1 and 6b2. Based on the helical field line structure, five flux ropes are identified in the RD current layer at $t = 55 \Omega_{i0}^{-1}$, as seen in Figures 6a1 and 6a2. Note that the flux rope "FR$_1$" inside the RD illustrated by the red field lines had formed around the Q-$\perp$ shock as described earlier. Four new flux ropes, denoted by white labels "FR$_2$" to "FR$_5$" have successively formed around the bow shock from $t = 50 \Omega_{i0}^{-1}$ to $t = 55 \Omega_{i0}^{-1}$, as the RD crosses different z locations of the Q-$\perp$ bow shock. In the meantime, the length of the flux ropes in the y direction becomes longer. For example, the length of "FR$_1$" is $\sim 15 d_{i0}$ around the Q-$\perp$ shock at $t = 50 \Omega_{i0}^{-1}$, while it increases to $\sim 30 d_{i0}$ in the Q-$\perp$ magnetosheath. Our simulation demonstrates that more reconnection sites form in the RD current layer after the RD crosses the Q-$\perp$ shock and propagates in the magnetosheath.

At $t = 60 \Omega_{i0}^{-1}$, four more flux ropes are present, as shown in Figures 6b1 and 6b2, denoted by the violet labels "FR$_6$" to "FR$_9$." Among them, "FR$_8$" and "FR$_9$" were initially formed by reconnection at the Q-$\perp$ shock. "FR$_6$" and "FR$_7$," on the other hand, are newly generated inside the RD by reconnection at new sites in the Q-$\perp$ magnetosheath. The flux ropes move tailward and poleward with the magnetosheath flows on both sides of the equator. For example, "FR$_1$" denoted by the red field lines is centered around $(x, z) = (12.73, -1.03) B_0$ at $t = 50 \Omega_{i0}^{-1}$ (Figures 3c and 3f) and has moved southward and tailward to $(x, z) = (11.83, -1.30) R_E$ at $t = 55 \Omega_{i0}^{-1}$ (Figure 6a). It then moves to $(x, z) = (11.12, -1.91) R_E$ at $t = 60 \Omega_{i0}^{-1}$ (Figure 6b). The average speed of "FR$_1$" is found to be consistent with the local magnetosheath flow speed. The flux ropes then propagate in the magnetosheath and eventually leave the tailward simulation boundary. This process has been investigated in our previous hybrid simulation studies of magnetosheath flux ropes (Guo et al., 2018, 2021b). Noted that no reconnection is found outside the RD in the magnetosheath.

### 3.2. Magnetopause Reconnection Associated With the Southward IMF Behind the RD

After the RD passes through the dayside magnetopause, several flux ropes are found to form by magnetopause reconnection under the southward IMF behind the RD. Figure 7 depicts the perspective views of three magnetopause flux ropes, overlaid on a snapshot of the field strength B in the $y = 0$ plane at $t = 100 \Omega_{i0}^{-1}$. The three flux ropes (red lines) "FR1," "FR2," and "FR3" in an enlarged view are displayed in Figures 7b–7d, respectively. The black field line is the northward magnetopause field line, and the arrows attached to the field lines denote the directions of the magnetic field. At $t = 100 \Omega_{i0}^{-1}$, the RD has completely passed through the low- and mid-latitudes of the magnetopause, and the IMF in the vicinity of these regions has changed to southward. As the southward IMF interacts with the northward magnetopause field, the three magnetopause flux ropes in Figures 7b–7d are present due to the magnetopause reconnection. The 3D structure of the magnetopause reconnection under a southward IMF has been studied by previous global hybrid simulations (e.g., Guo et al., 2020, 2021a, 2021b; Tan et al., 2011; Wang et al., 2019).

4. Conclusions and Discussion

In this paper, we have investigated the generation of ion-scale reconnection during the interaction of an interplanetary RD of half-width $\sim 1 d_{i0}$ with the Q-$\perp$ shock/magnetosphere using 3D global hybrid simulations. The initial IMF upstream (earthward) of the RD is assumed to have a predominant northward component. The magnetic field direction changes by 180° across the RD, and the propagation direction of the RD is nearly parallel to the $-x$ direction. The results are summarized as follows.

1. As the RD interacts with the Q-$\perp$ shock, the field line configuration on both sides of the RD changes due to the shock compression process. The current density of the RD increases by a factor of ~ 10 at the Q-$\perp$ shock
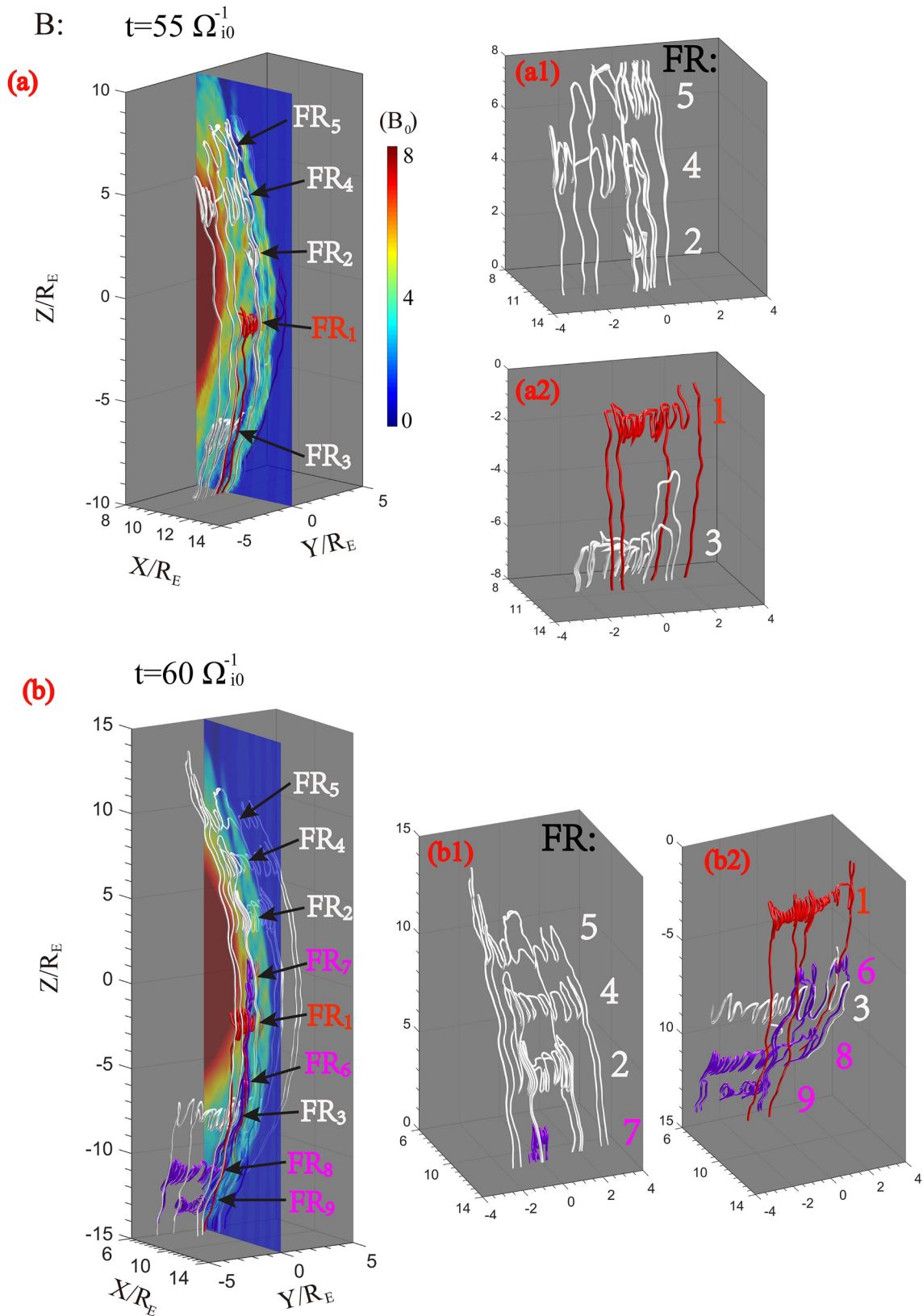
Figure 6. Contour plots of magnetic field strength B in the $y = 0$ plane at (a) $t = 55\Omega_{i0}^{-1}$ and (b) $t = 60\Omega_{i0}^{-1}$. The color lines superimposed on the contours denote the magnetic field lines of the flux ropes. (a1 and a2) and (b1 and b2) A zoom-in view.
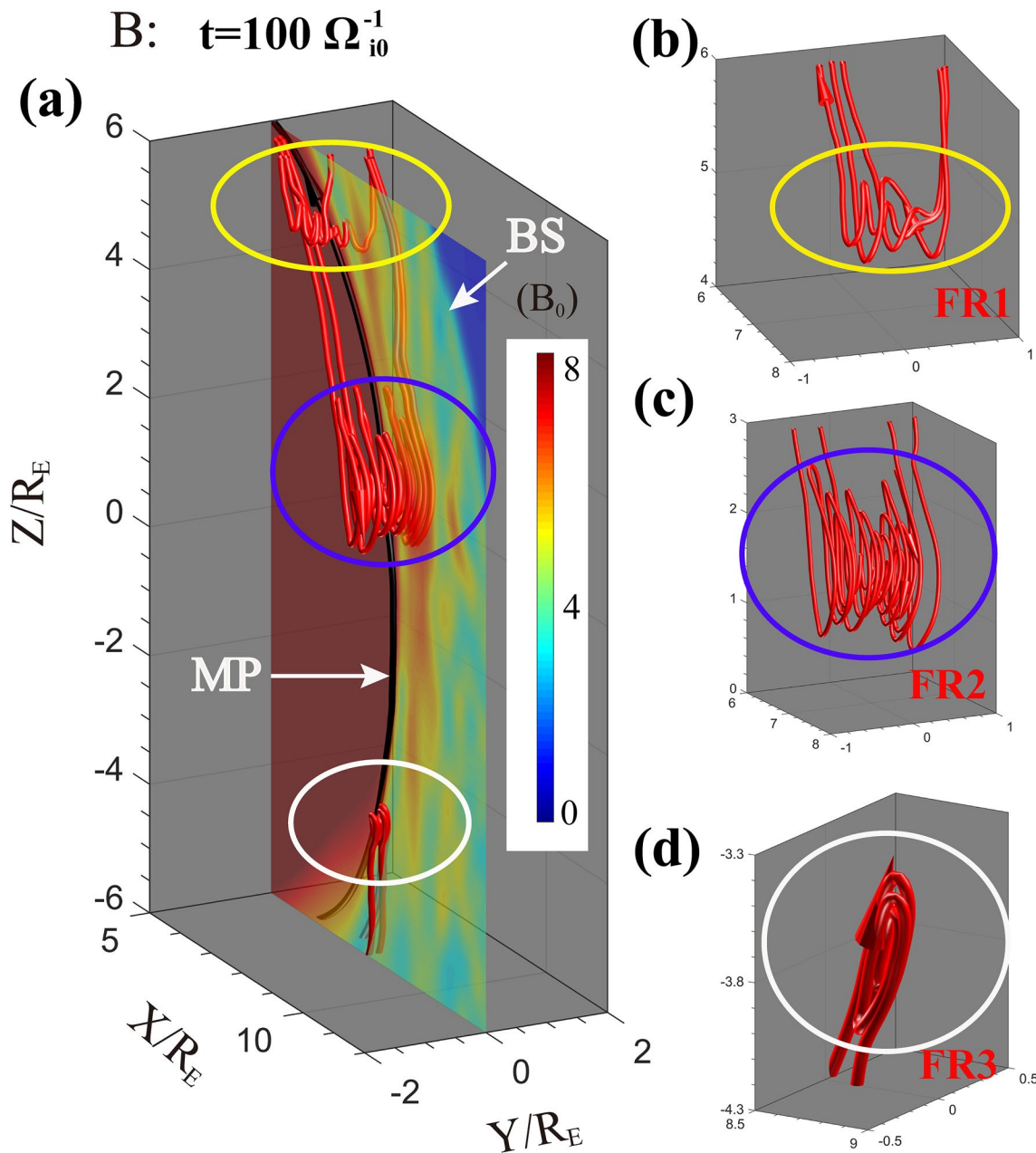
Figure 7. (a) Perspective views of the three magnetopause flux ropes, as well as the magnetic field strength B in the $y = 0$ plane, at $t = 100\Omega_{i0}^{-1}$. (b–d) The three flux ropes (red lines) "FR1," "FR2," and "FR3" in a zoom-in view.

from its value in the solar wind. A local thin current sheet with normal magnetic field $B_n \approx 0$ is created in the thinned RD.

2. Magnetic reconnection with a rate of ~0.1 takes place in the thin current sheet in the RD current layer as a result of its interaction with the Q-⊥ bow shock. Magnetic flux ropes form with a length of ~$15d_{i0}$ in the dawn-dusk direction at the Q-⊥ shock as the result of reconnection.

3. After the RD enters the magnetosheath through the Q-⊥ shock, more reconnection sites are seen in the RD current layer. The length of the flux ropes generated at the Q-⊥ shock due to multiple X points increase to tens of d_{i0}. During the subsequent evolution, more new reconnection sites are generated in the RD in the Q-⊥ magnetosheath. The flux ropes propagate poleward and tailward with the magnetosheath flow before leaving the dayside simulation domain

4. As the RD propagates across the magnetopause, the southward magnetic field behind the RD causes reconnection at the dayside magnetopause. Magnetopause flux ropes with a length of $\sim 2 - 20 d_{i0}$ form by the magnetopause reconnection

Our simulations show that ion-scale reconnection can occur in the RD current layer as it impacts the Q-⊥ shock and the magnetosheath. Similar reconnection events have been observed by MMS and Cluster spacecraft (Hamrin et al., 2019). Hamrin et al. (2019) reported that reconnection inside a DD at a Q-⊥ bow shock takes place as a non-reconnecting interplanetary DD is compressed at the Q-⊥ shock. Similar to our simulations, the observed DD in the above events has an almost 180° field rotation, and its propagation direction is nearly along the $-x$ direction. While it may be difficult to determine whether the DD is a TD or RD in the observations, and magnetosheath reconnection may be due to the impacts from a TD (Guo et al., 2018, 2021a; Omidi et al., 2009; Pang et al., 2010; Phan et al., 2007), our present simulation illustrates clearly reconnection can also be triggered in a large-amplitude RD after it is compressed by the bow shock. Note that we have also studied the effects of θ_{12} on reconnection inside the RD. It is found when θ_{12} is less than 135°, such reconnection can hardly be present. We suggest that the angle θ_{12} of the RD plays an important role in the triggering of reconnection in the RD current layer.

Previous hybrid simulation of Lin (1997) suggested no reconnection is present in an RD as it interacts with the bow shock. The simulation was based on a 2D model, and the field rotation angle $\Delta\Phi$ was 160°. In our present 3D global hybrid simulation, the rotation angle $\Delta\Phi$ is 180°. Magnetic reconnection is found inside the thinned RD current layer in both the Q-⊥ bow shock and the magnetosheath. Further investigations are necessary to understand the effects of $\Delta\Phi$ of the RD on the triggering of reconnection.

Besides the present study for the Q-⊥ bow shock geometry, our previous hybrid simulation (Guo et al., 2021b) found that ion-scale magnetic reconnection can also be triggered inside the RD current layer as it interacts with the Q-∥ bow shock and magnetosheath due to the existence of the large-amplitude magnetic fluctuations around the Q-∥ shock. The hybrid simulation does not include electron kinetic physics because it treats electrons as a massless fluid. Using 2D local particle-in-cell (PIC) simulations, electron-scale reconnection has been investigated for the Q-∥ shock (Bessho et al., 2019) and the Q-⊥ shock (Lu et al., 2021). Bessho et al. (2019) found that reconnection on the electron scale occurs in the Q-∥ shock transition and downstream regions, which is due to the interaction between the large-amplitude magnetic fluctuations with the rippled shock front. Lu et al. (2021) showed that electron-scale reconnection is present downstream of the Q-⊥ shock due to the squeezing of the magnetic field lines during the reformation of the shock. In addition, the PIC simulation of Bessho et al. (2019) showed that ion-scale reconnection takes place in the Q-∥ shock transition. The simulation was performed for a 2D local Q-∥ shock alone in slab geometry. In our simulation, however, no ion-scale reconnection is found in either the Q-∥ or Q-⊥ bow shock outside the RD. While our simulation includes the 3D global geometry together with the ion-kinetic scale physics, its spatial resolution is not as high as local simulations. More global simulations are necessary to investigate the effects of grid resolution, including the effects of d_{i0} used in the simulation (e.g., compare with the runs using a smaller d_{i0}; Guo et al., 2018).

Data Availability Statement

The simulation data sets for this research are available via figshare (https://doi.org/10.6084/m9.figshare.16594949.v2).

References

Behannon, K. W., Neubauer, F. M., & Barnstorf, H. (1981). Fine-scale characteristics of interplanetary sector boundaries. *Journal of Geophysical Research*, *86*, 3273–3287. https://doi.org/10.1029/JA086iA05p03273

Bessho, N., Chen, L. J., Wang, S., Hesse, M., & Wilson, L. B. (2019). Magnetic reconnection in a quasi-parallel shock: Two-dimensional local particle-in-cell simulation. *Geophysical Research Letters*, *46*, 9352–9361. https://doi.org/10.1029/2019GL083397

Birn, J., Borovsky, J. E., & Hesse, M. (2008). Properties of asymmetric magnetic reconnection. *Physics of Plasmas*, *15*(3), 32101. https://doi.org/10.1063/1.2888491

Burch, J. L., Moore, T. E., Torbert, R. B., & Giles, B. L. (2016). Magnetospheric Multiscale overview and science objectives. *Space Science Reviews*, *199*, 5–21. https://doi.org/10.1007/s11214-015-0164-9

Burlaga, L. F., Lemaire, J. F., & Turner, J. M. (1977). Interplanetary current sheets at 1 AU. *Journal of Geophysical Research*, *82*, 3191–3200. https://doi.org/10.1029/JA082i022p03191

Cooling, B. M. A., Owen, C. J., & Schwartz, S. J. (2001). Role of the magnetosheath flow in determining the motion of open flux tubes. *Journal of Geophysical Research*, *106*, 18763–18775. https://doi.org/10.1029/2000JA000455

Dungey, J. W. (1961). Interplanetary magnetic field and the auroral zones. *Physical Review Letters*, *6*(2), 47–48. https://doi.org/10.1103/PhysRevLett.6.47

Eastwood, J. P., Lucek, E. A., Mazelle, C., Meziane, K., Narita, Y., Pickett, J., & Treumann, R. A. (2005). The foreshock. *Space Science Reviews* *118*, 41–94. https://doi.org/10.1007/s11214-005-3824-3

Eastwood, J. P., Mistry, R., Phan, T. D., Schwartz, S. J., Ergun, R. E., Drake, J. F., et al. (2018). Guide field reconnection: Exhaust structure and heating. *Geophysical Research Letters*, *45*, 4569–4577. https://doi.org/10.1029/2018gl077670

Fuselier, S. A., Trattner, K. J., Petrinec, S. M., & Lavraud, B. (2012). Dayside magnetic topology at the Earth's magnetopause for northward IMF. *Journal of Geophysical Research*, *117*, A08235. https://doi.org/10.1029/2012JA017852

Gingell, I., Schwartz, S. J., Eastwood, J. P., Burch, J. L., Ergun, R. E., Fuselier, S., et al. (2019). Observations of Magnetic reconnection in the transition region of quasi-parallel shocks. *Geophysical Research Letters*, *46*, 1177–1184. https://doi.org/10.1029/2018gl081804

Guo, J., Lu, S., Lu, Q., Lin, Y., Wang, X., Huang, K., et al. (2021). Structure and Coalescebce of Magnetopause Flux ropes and Their Dependence on IMF Clock Angle: Three-Dimensional Global Hybrid Simulations. *Journal of Geophysical Research*, *126*, e2020JA028670. https://doi.org/10.1029/2020ja028670

Guo, Z., Lin, Y., & Wang, X. (2021a). Investigation of the interaction between magnetosheath reconnection and magnetopause reconnection driven by oblique interplanetary tangential discontinuity using three-dimensional global hybrid simulation. *Journal of Geophysical Research*, *126*, e2020JA028558. https://doi.org/10.1029/2020ja028558

Guo, Z., Lin, Y., & Wang, X. (2021b). Global hybrid simulations of interaction between interplanetary rotational discontinuity and bow shock/magnetosphere: Can ion-scale magnetic reconnection be driven by rotational discontinuity downstream of quasi-parallel shock? *Journal of Geophysical Research*, *126*, e2020JA028853. https://doi.org/10.1029/2020ja028853

Guo, Z., Lin, Y., Wang, X., & Du, A. (2018). Magnetosheath reconnection before magnetopause reconnection driven by interplanetary tangential discontinuity: A three-dimensional global hybrid simulation with oblique interplanetary magnetic field. *Journal of Geophysical Research*, *123*, 9169–9186. https://doi.org/10.1029/2018ja025679

Guo, Z., Lin, Y., Wang, X., Vines, S. K., Lee, S. H., & Chen, Y. (2020). Magnetopause reconnection as influenced by the dipole tilt under southward IMF conditions: Hybrid simulation and MMS observation. *Journal of Geophysical Research*, *125*, e2020JA027795. https://doi.org/10.1029/2020ja027795

Hamrin, M., Gunell, H., Goncharov, O., De Spiegeleer, A., Fuselier, S., Mukherjee, J., et al. (2019). Can reconnection be triggered as a solar wind directional discontinuity crosses the bow shock? A case of asymmetric reconnection. *Journal of Geophysical Research*, *124*, 8507, 8523. https://doi.org/10.1029/2019JA027006

Hasegawa, H., Wang, J., Dunlop, M. W., Pu, Z. Y., Zhang, Q.-H., Lavraud, B., et al. (2010). Evidence for a flux transfer event generated by multiple X-line reconnection at the magnetopause. *Geophysical Research Letters*, *37*, L16101. https://doi.org/10.1029/2010GL044219

Kropotina, A., Lee, W., Artemyev, A. V., Bykov, A. M., Vainchtein, D. L., & Vasko, I. Y. (2021). Solar wind discontinuity Transformation at the bow shock. *The Astrophysical Journal*, *913*, 142. https://doi.org/10.3847/1538-4357/abf6c7

Lee, G., & Russell, C. T. (1994). The morphology of ULF waves in the Earth's foreshock. In M. J. Engebretson, K. Takahashi, M. Scholer (Eds.), *Solar wind sources of magnetospheric ultra low-frequency waves. Geophysical Monograph Series* (81, pp. 87–98). AGU.

Lepping, R. P., & Behannon, K. W. (1986). Magnetic field directional discontinuities: Characteristics between 0.46 and 1.0 AU. *Journal of Geophysical Research*, *91*, 8725–8741. https://doi.org/10.1029/JA091iA08p08725

Lin, Y. (1997). Generation of anomalous flows near the bow shock by its interaction with interplanetary discontinuities. *Journal of Geophysical Research*, *102*, 24265–24281. https://doi.org/10.21236/ada635320

Lin, Y., & Wang, X. (2005). Three-dimensional global hybrid simulation of dayside dynamics associated with the quasi-parallel bow shock. *Journal of Geophysical Research*, *110*, A12216. https://doi.org/10.1029/2005ja011243

Lin, Y., Wang, X., Lu, S., Perez, J. D., & Lu, Q. (2014). Investigation of storm time magnetotail and ion injection using three-dimensional global hybrid simulation. *Journal of Geophysical Research: Space Physics*, *119*, 7413–7432. https://doi.org/10.1002/2014JA020005

Liu, T. Z., Lu, S., Angelopoulos, V., Lin, Y., & Wang, X. Y. (2018). Ion acceleration inside foreshock transients. *Journal of Geophysical Research: Space Physics*, *23*, 163–178. https://doi.org/10.1002/2017ja024838

Lu, Q., Wang, H., Wang, X., Lu, S., Wang, R., Gao, X., & Wang, S. (2020). Turbulence-driven magnetic reconnection in the magnetosheath downstream of a quasi-parallel shock: A three-dimensional global hybrid simulation. *Geophysical Research Letters*, *47*, e2019GL085661. https://doi.org/10.1029/2019GL085661

Lu, Q., Yang, Z., Wang, H., Wang, R., Huang, K., Lu, S., & Wang, S. (2021). Two-dimensional particle-in-cell simulation of magnetic reconnection in the downstream of a quasi-perpendicular shock. *The Astrophysical Journal*, *919*, 28. https://doi.org/10.3847/1538-4357/ac18c0

Maynard, N. C., Burke, W. J., Ober, D. M., Farrugia, C. J., Kucharek, H., Lester, M., et al. (2007). Interaction of the bow shock with a tangential discontinuity and solar wind density decrease: Observations of predicted fast mode waves and magnetosheath merging. *Journal of Geophysical Research*, *112*, A12219. https://doi.org/10.1029/2007JA012293

Moore, T. E., Fok, M.-C., & Chandler, M. O. (2002). The dayside reconnection X line. *Journal of Geophysical Research*, *107*, 1332. https://doi.org/10.1029/2002JA009381

Mozer, F. S., Bale, S. D., & Phan, T. D. (2002). Evidence of diffusion regions at a subsolar magnetopause crossing. *Physical Review Letters*, *89*(1), 015002. https://doi.org/10.1103/PhysRevLett.89.015002

Øieroset, M., Phan, T., Shay, M. A., Haggerty, C. C., Fujimoto, M., Angelopoulos, V. J., et al. (2017). THEMIS multispacecraft observations of a reconnecting magnetosheath current sheet with symmetric boundary conditions and a large guide field. *Geophysical Research Letters*, *44*, 7598–7606.

Omidi, N., Phan, T., & Sibeck, D. G. (2009). Hybrid simulations of magnetic reconnection initiated in the magnetosheath. *Journal of Geophysical Research*, *114*, A02222. https://doi.org/10.1029/2008ja013647

Onsager, T. G., Scudder, J. D., Lockwood, M., & Russell, C. T. (2001). Reconnection at the high-latitude magnetopause during northward interplanetary magnetic field conditions. *Journal of Geophysical Research*, *106*(A11), 25467–25488. https://doi.org/10.1029/2000JA000444

Pang, Y., Lin, Y., Deng, X. H., Wang, X. Y., & Tan, B. (2010). Three-dimensional hybrid simulation of magnetosheath reconnection under northward and southward interplanetary magnetic field. *Journal of Geophysical Research*, *115*, A03203. https://doi.org/10.1029/2009ja014415

Paschmann, G., Papamastorakis, I., Sckopke, N., Sckopke, N., Haerendel, G., Bame, S. J., et al. (1979). Plasma acceleration at the Earth's magnetopause-evidence for reconnection. *Nature*, *282*, 243–246. https://doi.org/10.1038/282243a0

Phan, T., Dunlop, M., Paschmann, G., Klecker, B., Bosqued, J. M., Rème, H., et al. (2004). Cluster observations of continuous reconnection at the magnetopause under steady interplanetary magnetic field conditions. *Annales Geophysicae*, *22*, 2355–2367. https://doi.org/10.5194/angeo-22-2355-2004

Phan, T., Eastwood, J. P., Shay, M. A., Drake, J. F., Sonnerup, B. U. Ö., Fujimoto, M., et al. (2018). Electron magnetic reconnection without ion coupling in Earth's turbulent magnetosheath. *Nature*, *557*, 202, 206. https://doi.org/10.1038/s41586-018-0091-5

Phan, T., Love, T. E., Gosling, J. T., Paschmann, G., Eastwood, J. P., Oieroset, M., et al. (2011). Triggering of magnetic reconnection in a magnetosheath current sheet due to compression against the magnetopause. *Geophysical Research Letters*, *38*, L17101. https://doi.org/10.1029/2011GL048586

Phan, T., Paschmann, G., Twitty, C., Mozer, F. S., Gosling, J. T., Eastwood, J. P., et al. (2007). Evidence for magnetic reconnection initiated in the magnetosheath. *Geophysical Research Letters*, *34*, L14104. https://doi.org/10.1029/2007GL030343

Pritchett, P. L. (2001). Geospace environment modeling magnetic reconnection challenge: Simulations with a full particle electromagnetic code. *Journal of Geophysical Research*, *106*(A3), 3783–3798. https://doi.org/10.1029/1999JA001006

Pritchett, P. L. (2008). Collisionless magnetic reconnection in an asymmetric current sheet. *Journal of Geophysical Research*, *113*, A06210. https://doi.org/10.1029/2007JA012930

Retinò, A., Sundkvist, D., Vaivads, A., Mozer, F., André, M., & Owen, C. J. (2007). In situ evidence of magnetic reconnection in turbulent plasma. *Nature Physics*, *3*, 235–238.

Sonnerup, B. U. Ö., Paschmann, G., Papamastorakis, I., Sckopke, N., Haerendel, G., Bame, S. J., et al. (1981). Evidence for magnetic field reconnection at the Earth's magnetopause. *Journal of Geophysical Research*, *86*, 10049-10067. https://doi.org/10.1029/JA086iA12p10049

Swift, D. W. (1996). Use of a hybrid code for global-scale plasma simulation. *Journal of Computational Physics*, *126*(109), 121. https://doi.org/10.1006/jcph.1996.0124

Tan, B., Lin, Y., Perez, J. D., & Wang, X. (2011). Global-scale hybrid simulation of dayside magnetic reconnection under southward IMF: Structure and evolution of reconnection. *Journal of Geophysical Research*, *116*, A02206. https://doi.org/10.1029/2010ja015580

Trattner, K. J., Mulcock, J., Petrinec, S. M., & Fuselier, S. A. (2007). The location of the reconnection line at the magnetopause during southward IMF conditions. *Geophysical Research Letters*, *34*, L03108. https://doi.org/10.1029/2006GL028397

Tsurutani, B. T., & Smith, E. F. (1979). Interplanetary discontinuities: Temporal variations and the radial gradient from 1 to 8.5 AU. *Journal of Geophysical Research*, *84*, 2773–2787. https://doi.org/10.1029/JA084iA06p02773

Vörös, Z., Yordanova, E., Varsani, A., Genestreti, K. J., Khotyaintsev, Y. V., Li, W., et al. (2017). MMS observation of magnetic reconnection in the turbulent magnetosheath. *Journal of Geophysical Research: Space Physics*, *122*, 11-442.

Wang, H., Lin, Y., Wang, X., & Guo, Z. (2019). Generation of kinetic Alfvén waves in dayside magnetopause reconnection: A 3-D global scale hybrid simulation. *Physics of Plasmas*, *26*, 072102. https://doi.org/10.1063/1.5092561

Wang, S., Chen, L.-J., Bessho, N., Yao, Z. H., Fu, H. S., Degeling, A. W., et al. (2018). Observational evidence of magnetic reconnection in the terrestrial bow shock transition region. *Geophysical Research Letters*, *46*, 562–570.

Yao, S., Shi, Q., Guo, R., Yao, Z., Fu, H., Degeling, A., et al. (2020). Kinetic-scale Flux Rope in the magnetosheath Boundary Layer. *The Astrophysical Journal*, *897*(2), 137. https://doi.org/10.3847/1538-4357/ab9620

Yordanova, E., Vörös, Z., Varsani, A., Graham, D. B., Norgren, C., Khotyaintsev, Y. V., et al. (2016). Electron scale structures and magnetic reconnection signatures in the turbulent magnetosheath. *Geophysical Research Letters*, *43*, 5969, 5978. https://doi.org/10.1002/2016gl069191